Supporting Information

Enhanced Thermal Conductivity of Liquid Crystalline Epoxy Resin using Controlled Linear Polymerization

Akherul Md. Islam[1,3], Hongjin Lim[1], Nam-Ho You[2], Seokhoon Ahn[1], Munju Goh[2], Jae Ryang Hahn[3,], Hyeonuk Yeo[4,*], Se Gyu Jang[1,*]*

[1] Functional Composite Materials Research Center, [2] Carbon Composite Materials Research Center, Institute of Advanced Composites Materials, Korea Institute of Science and Technology, Wanju, Jeonbuk, 565-905, Republic of Korea, [3] Department of Chemistry and Department of Bioactive Material Sciences and Research Institute of Physics and Chemistry, Chonbuk National University, Jeonju, Jeonbuk, 561-756, Republic of Korea [4] Department of Chemistry Education, Kyungpook National University, Daegu 41566, Republic of Korea

1. Materials and methods

Materials. All commercial reagents, i.e., 4,4′-biphenol (Wako Chemical Co.), benzyltrimethylammonium bromide (Sigma-Aldrich), 4,4′-diaminodiphenylsulfone (Kukdo Chemical), epichlorohydrin (Daejung), pyrazine (Alfa Aesar), benzyl bromide (Alfa Aesar), and sodium hexafluoroantimonate (V) (Alfa Aesar) were used as received. Boron nitride platelets, BN-XGP (~30 μm diameter) were purchased from Denka (Japan).

Synthesis of the LC epoxy resin. 4,4′-Biphenol (114.5 g, 614.9 mmol) and benzyltrimethyl-ammonium bromide (4.2 g, 18.2 mmol) were added to epichlorohydrin (1 L) in a three-necked round bottomed flask under magnetic stirring at 25 °C.[1] After heating at 110 °C for 30 min, a solution of sodium hydroxide (4.0 M, 308 mL) was added dropwise to the flask over 1 h, and the resulting solution was stirred for a further 1 h prior to cooling to room temperature (25 °C). Following removal of the remaining epichlorohydrin and water by vacuum distillation, the obtained white powder was washed with deionized (DI) water (×3) and dried in a vacuum oven (175.3 g, 95.4%). The epoxy equivalent weight (EEW) of the LCER was ~190 g/eq. ^{1}H NMR (DMSO-d_6, ppm) 7.55 (m, Ar–*H*), 7.02 (m, Ar–*H*), 5.45 (m, R–O*H*), 4.36 (m, ArOCH_2–epoxide), 4.25–4.00 (m, ArCH_2–C*H*OH–CH_2Ar), 3.85 (m, OCH_2–epoxide), 3.35 (m, R–C*H*OCH$_2$), 2.85 (m, R–CHOCH_2), 2.72 (m, R–CHOCH_2).

Synthesis of the cationic initiator. The cationic initiator, *N*-benzylpyrazinium hexafluoroantimonate, was synthesized according to a modified literature procedure.[2] More specifically, pyrazine (1.6 g, 20 mmol) and benzyl bromide (7.3 g, 42.7 mmol) were added to a 250 mL round bottomed flask agitated by a mechanical stirrer at room temperature. After 1 d, the white precipitate was filtered and washed with diethyl ether (×3). After drying under vacuum, the obtained powder was added to a fresh aqueous solution of $NaSbF_6$ (5.17 g in

30 mL water, 20 mmol) under stirring. The resulting white precipitate was filtered and dried under vacuum prior to recrystallization from methanol to give the desired product (4.5 g, 55.3%).

Preparation of the epoxy composites. The LCER composites were prepared using a dry hot-pressing method.[1] Initially, the LCER, curing agents, and h-BN fillers were mixed and ground using a Lab Mill equipped with a 100-μm sieve, then mixed further using a Thinky mixer. The resulting powder was subsequently inserted into a cylindrical SUS mold (2 mm diameter) and heated to 170 °C to cure the composites under 20 MPa pressure. Curing times of 2 and 1 h were used for the 4,4-DDS- and BPH-cured composites, respectively.

Characterization. The ^{1}H NMR spectra were measured using a 600 MHz Premium COMPACT NMR spectrometer (Agilent, USA) with tetramethylsilane (TMS) as the internal standard and DMSO-d_6 as the solvent. The glass transition temperatures (T_g), liquid crystalline behaviors, and curing properties of the epoxy resins were determined by differential scanning calorimetry (DSC, Auto-Q20, TA Instruments, USA) under a flow of nitrogen gas at a heating rate of either 10 or 20 °C/min. Microscopic observations were carried out under crossed Nicols using a Carl Zeiss AXIO IMAGER MIM polarizing optical microscope (POM) equipped with a Linkam TH-600PM and a L-600 temperature-controlled stage. Thermal conductivities were recorded using a Hot Disk TPS 2500 S model with #7531 or #7577 Kapton sensors (Hot Disk, Sweden) according to the ISO standard 22007-2. In addition, the specimens were prepared as round chips (20 mm diameter, >3 mm thickness) to measure their thermal conductivities. (see supporting information S7 for detailed theory related to the measurements) For powder grinding and mixing, a Lab Mill PX-MFC 90 D equipped with a hammer mill (Kinematica, Germany) and a planetary centrifugal mixer (AR-100, Thinky, Japan) were employed. XRD data were obtained using a Rigaku SmartLab with

Cu K_α radiation. Cross-sectional morphologies of the epoxy composites were observed by field-emission scanning electron microscopy (FE-SEM, NOVA NanoSEM 450, FEI, USA). Furthermore, the densities of the composites were calculated using the Archimedes principle (ASTM D 792-91) with a density kit and an XS204 balance (Mettler Toledo, Switzerland). Finally, the thermomechanical behaviors of the specimens were evaluated under air using a dynamic mechanical thermal analyzer (DMA, TA Instruments, DMA Q800, USA) at a heating rate of 3 °C/min with a load frequency of 1 Hz using a dual cantilever clamp for the rectangular sample.

Supporting Information S1. Figure S1

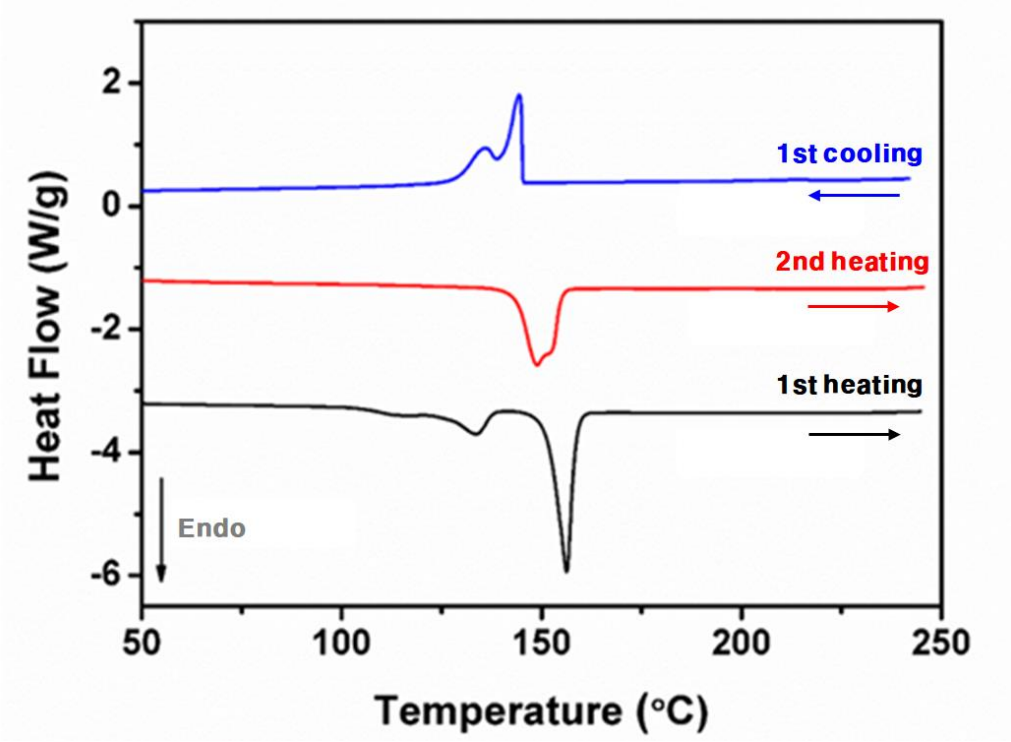

Figure S1. DSC graphs of the BP-based LCER showing thermal phase transitions

Supporting Information S2. Discussion on DMA analysis and Figure S2

To address thermomechanical properties of the neat LCER and h-BN composites, dynamic mechanical analysis (DMA) was carried out with the neat DDS-cured LCER as a reference (Figure S2). In the low temperature region, the storage modulus of the neat BPH-cured LCER (3 wt%, black lines) was comparable to the one of the DDS-cured LCER (blue lines), indicating that good mechanical property of LCER can be obtained via cationic curing system. In the high temperature region, especially over T_g, the BPH-cured LCER showed a higher storage modulus value than the DDS-cured one. This observation reflects that curing with BPH induces higher crosslink density than the DDS considering that the higher storage modulus at rubbery plateau means the higher crosslink density. To be specific, the crosslink density values can be calculated by the following equation;[3]

$$\rho = \frac{G'}{RT}$$

where ρ means the crosslink density in mol/cm^3, G' is storage modulus measured in rubbery region, R is universal gas constant (8.3145 J K^{-1} mol^{-1}), T is absolute temperature. At 250 °C in the rubbery region, the calculated crosslink density of the BPH-cured LCER was 0.1025 mol/cm^3, which was more than ten times higher than the value of the DDS-cured one (0.0094 mol/cm^3). Although the T_g of the BPH-cured LCER obtained from Tan δ peak is 165 °C, which is lower than that of the 4,4'-DDS-cured one, it is still reasonably high value compared to the other common epoxy resins. In addition, from DMA analysis of LCER composites with h-BN (60 vol%, red lines), the similar tendency with the neat BPH-cured LCER was observed, indicating that excellent thermomechanical properties were also maintained even when preparing the composites with high volume fraction. Both of the storage modulus and

the loss modulus in the composite considerably increased compared to the neat LCER due to the increase in the volume fraction of h-BN having high modulus.

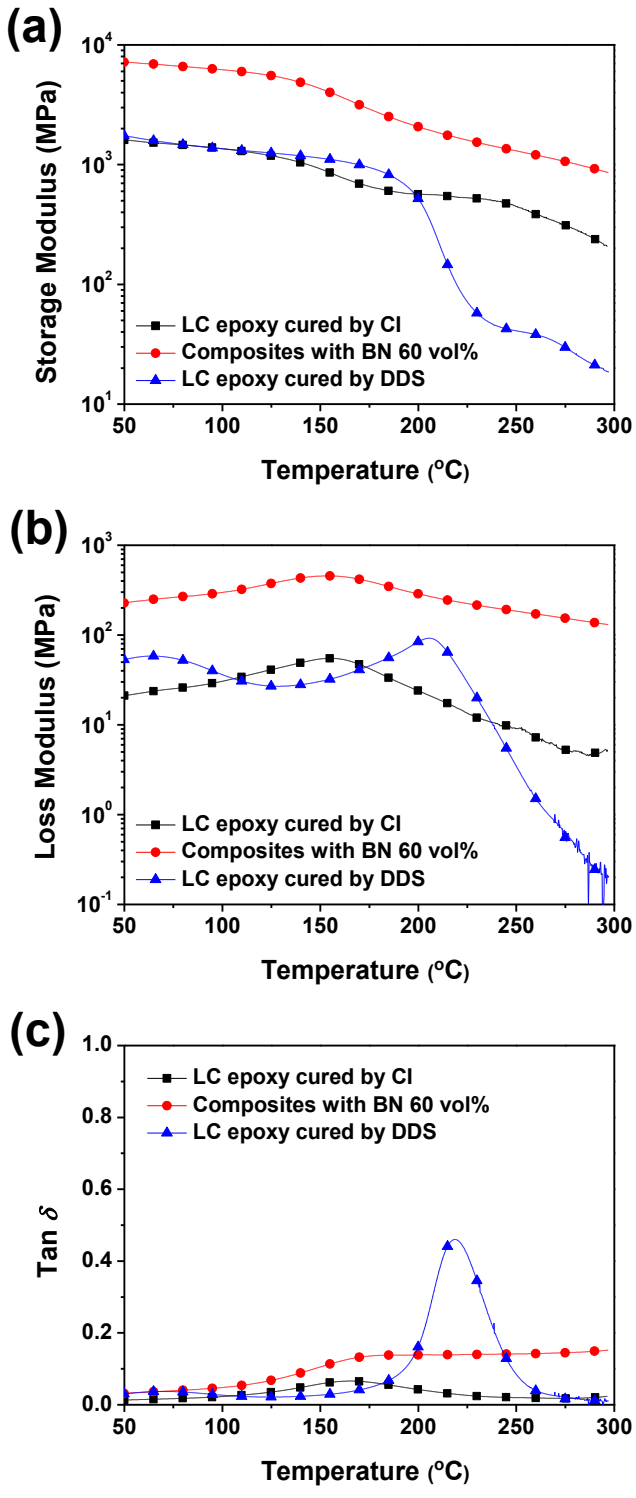

Figure S2. DMA curves of the neat LC epoxy resin (LCER) cured by two kinds of curing agents, BPH cationic initiator (CI) and DDS, and the composite with 60 vol% h-BN (1 Hz, heating rate: 3 °C/min); (a) storage modulus (E′), (b) loss modulus (E″), (c) tan δ.

Supporting Information S3. Discussion on isothermal DSC analysis and Figure S3-S5

To investigate the curing kinetics of BPH-cured LCER, the isothermal DSC curves at different temperatures (Figure S3) were converted to the differential curing rate ($d\alpha/dt$) and the degree of conversion (α) as a function of time as shown in Figure S4 and S5 according to the following equation;[4-6]

$$d\alpha/dt = (1/Q_T)(dQ/dt)$$

$$\alpha = Q/Q_T$$

where Q_T and Q mean the total curing heat and the cumulative heat at a time, respectively. Based on the analysis on cumulative curing heat and degree of conversion, it could be concluded that the complete curing could be achieved at temperatures above 165 °C. In a DSC pan scale (~10 mg), the full curing took approximately 45 min at 165 °C, 40 min at 170 °C, and 35 min at 180 °C. Considering the information above, the LCER was cured with BPH for an hour at 170 °C, which is in the range of LC-forming temperature window.

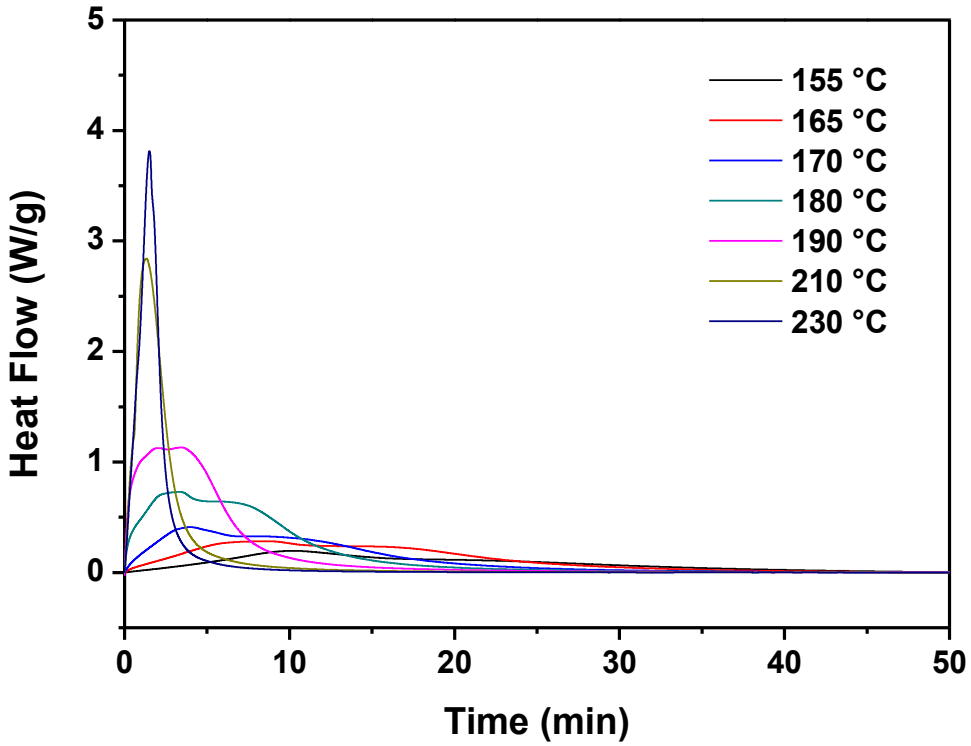

Figure S3. Isothermal DSC curves of LCER cured by cationic initiator (3 wt%) at different temperatures (under N_2 atmosphere).

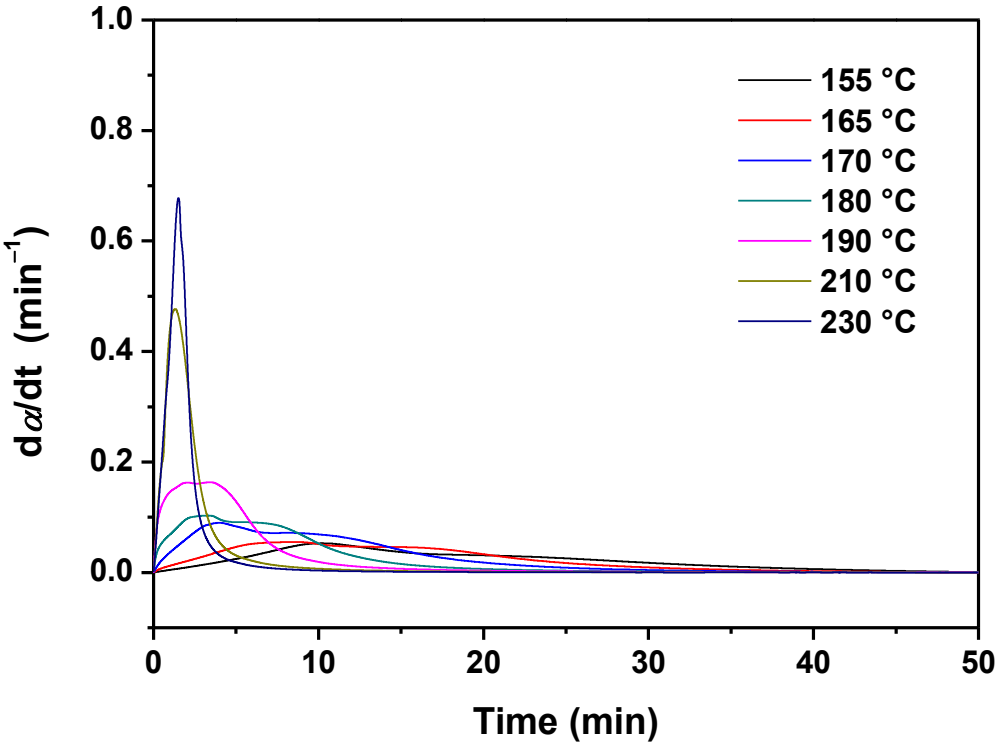

Figure S4. Curing reaction rate of LCER cured by cationic initiator (3 wt%) at different temperatures (under N_2 atmosphere).

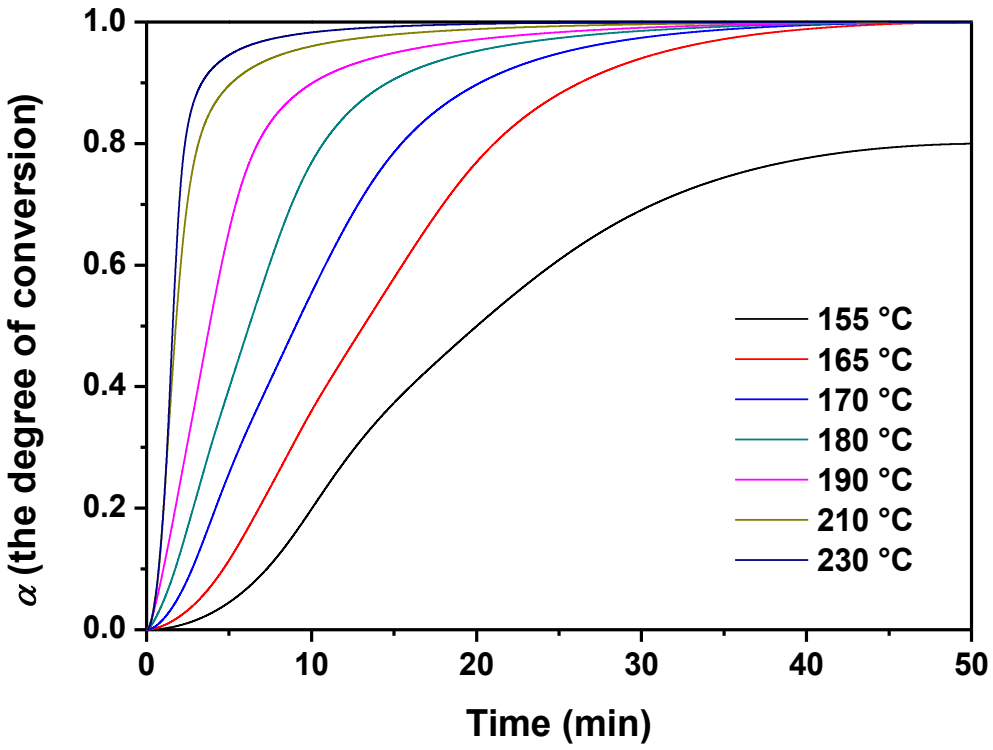

Figure S5. The degree of conversion of LCER cured by cationic initiator (3 wt%) at different temperatures (under N_2 atmosphere).

Supporting Information S4. A brief theoretical description of Hot Disk thermal constants analysis.

The Hot Disk Thermal Constants Analyser employed in this study is based on the Transient Plane Source (TPS) method which provides information on thermal conductivity, thermal diffusivity, and specific heat per unit volume in accordance with ISO 22007-2. For thermal conductivity measurement, a Hot Disk sensor, which is consisted of a double spiral nickel pattern, is heated by electrical current resulting in the temperature increase of specimens. The increase in temperature as a function of time is simultaneously recorded by the sensor. The characterization method is based on the assumption that the sensor is covered by the infinite sample medium meaning that there is no thermal interruption from the outside samples.

When the double spiral sensor is electrically heated, the total electrical resistance increases at time *t*, is given by:

$$\mathrm{R}(t) = R_0\ [1 + \alpha \Delta \bar{T}(t)]$$

where R_0 is the initial resistance of the disk at $t = 0$, α is the temperature coefficient of the resistivity for nickel.

From the theory,[7] the time-dependent average temperature increase in the double spiral sensor surface is described as:

$$\Delta \bar{T}(\tau) = \frac{P_0}{\pi^{\frac{2}{3}}\ r\ \lambda}\ D(\tau)$$

where P_0 is the total power from the sensor, r is the radius of the disk, λ is the thermal conductivity of the specimen. Therefore, a straight line is obtained by plotting $\Delta\bar{T}(\tau)$ as a function of $D(\tau)$ and the slop of the line is $P_0/(\pi^{\frac{2}{3}}\ r\ \lambda)$. From the slope, thermal conductivity of the specimen can be calculated. The dimensionless time function, $D(\tau)$, can be evaluated numerically with the dimensionless parameter τ ($\tau = \sqrt{\kappa t}/r$, where κ is thermal diffusivity of the specimen). The unknown thermal diffusivity can be numerically optimized by make a series of computational plots of $\Delta\bar{T}(\tau)$ vs $D(\tau)$ for a range of thermal diffusivity (κ) values. The data analysis program in Hot Disk Thermal Constants Analyser provides the plots of $\Delta\bar{T}(\tau)$ vs $D(\tau)$ for specimen and from the slope thermal conductivity can be calculated.

Supporting Information S5. Volume fraction measurement (Table S1)

Table S1. Measured void fractions of composite samples

Vol%	Density BP/CI/hBN (g/cm^3)		Void (%)	Density BP/DDS/h-BN (g/cm^3)		Void (%)
	Measured	*Calculated*		*Measured*	*Calculated*	
10	1.32	1.32	0	1.30	1.31	1
20	1.42	1.43	1	1.40	1.42	1
30	1.53	1.54	1	1.51	1.53	1
40	1.62	1.65	2	1.61	1.64	2
50	1.71	1.75	2	1.69	1.74	3
60	1.78	1.88	5	1.79	1.86	4

Supporting Information S6. Cross-sectional SEM images of composite samples (Figure S6)

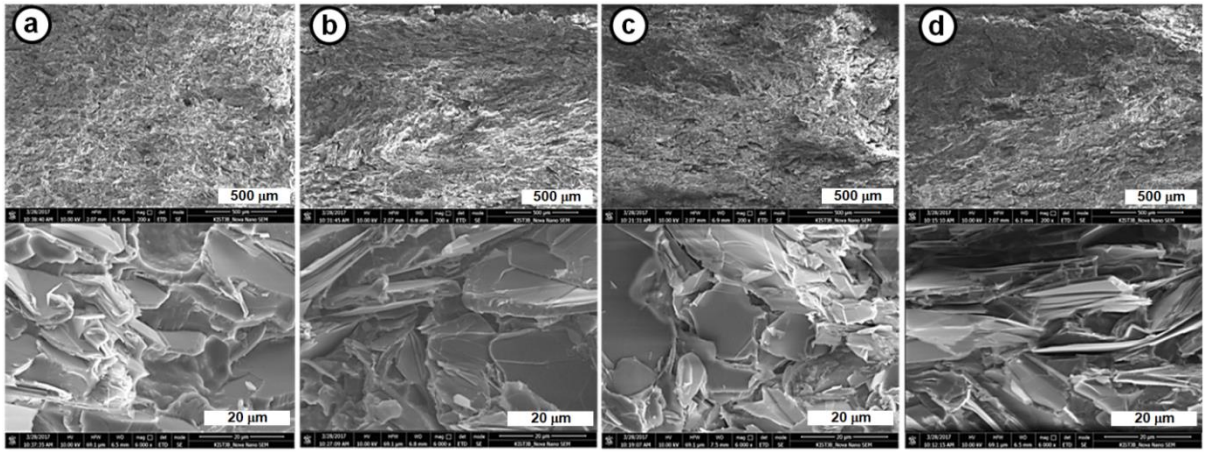

Figure S6. Cross-sectional SEM images of the BPH-cured LCER composites containing various volume fractions of hexagonal boron nitride (h-BN) platelets: (a) 30 vol%, (b) 40 vol%, (c) 50 vol%, and (d) 60 vol%. For preparation using the hot-pressing method, the pressure was applied from the top to the bottom of the images.

Supporting Information S7. Theoretical analysis on thermal conductivity of h-BN/LCER composites and Figure S7

To gain a deeper insight into the origin of the high thermal conductivity of the h-BN/BPH-cured LCER composites, the experimental results were analyzed using a theoretical model. Among the various models available, including the Agari,[8] Maxwell,[9] and Cheng-Vachon[10] models, the Nielsen model was adopted as it considers the orientation and aspect ratio of the fillers, which are important to understanding the thermal conduction behaviors of composites containing anisotropic h-BN platelets.[11–12] Thus, the thermal conductivities of these can be described according to the following equation:

$$\frac{K}{K_m} = \frac{1+AB\Phi}{1-\psi B\Phi}$$

where K and K_m are the thermal conductivities of the composite and the matrix resin, respectively. The geometry factor A, related to the filler anisotropicity and orientation, can be expressed by the generalized Einstein coefficient (P_E), which can be obtained by the Guth equation:[13]

$$A = P_E - 1$$

$$P_E = \frac{P}{2\ln(2P)-3} + 2$$

The parameter B is defined by the relative thermal conductivities of the filler (K_f) and the matrix (K_m) as follows:

$$B = \frac{\left(\frac{K_f}{K_m}\right)-1}{\left(\frac{K_f}{K_m}\right)+A}$$

while parameter ψ is a function of the volume fraction (Φ):

$$\psi = 1 + \frac{1-\Phi_m}{\Phi_m{}^2}\ \Phi$$

where Φ_m is the maximum filler volume fraction that maintains a continuous matrix. Setting the parameter A as ~6.8 with an average aspect ratio of the h-BN (P ~30), K_f ~400 W/mK (in-plane),[14] K_m ~0.48 W/mK, and an Φ_m of 0.8 (chosen value for the best fit of experimental data), the predicted thermal conductivity shown in Figure S7 (blue circles) was significantly lower than that obtained experimentally from the BPH-cured LCER/h-BN composites (filled red circles). The data fit well when the aspect ratio of the filler (P) was increased from 30 to 305 (A ~32), which is significantly higher than the experimental value (black open circles, Figure S7). This result indicates that conductive chain formation takes place in the h-BN platelets due to the large conformal contact area, which leads to a significant increase in the effective aspect ratio and a corresponding increase in the thermal conductivity.[15] Indeed, the thin plate-shaped morphology of h-BN is advantageous in the formation of large contact areas between the fillers due to its lubricious nature and facile deformation under the high pressure applied during composite fabrication.[16-17] To confirm the validity of this model, the empirical thermal conductivities of the DDS-cured LCER/h-BN composites were also fitted with the same parameters (Figure 5 in main text), with the exception of the thermal conductivity of the resin (K_m ~0.34 W/mK). The empirical data agreed well with the theoretical prediction, indicating that similar conductive chains of fillers are formed at equal filler contents regardless of the curing method employed. In both cases, low thermal conductivities were observed compared to the predicted values at high filler contents (60 vol%), likely due to inefficient mixing of the filler and an increase in the void fraction inside the composite (~5% for 60 vol%). The low thermal conductivity obtained at high filler contents can therefore likely be improved further by careful optimization of the mixing and

hot-pressing conditions, and also by employing advanced fabrication tools such as a vacuum-assisted hot-press.

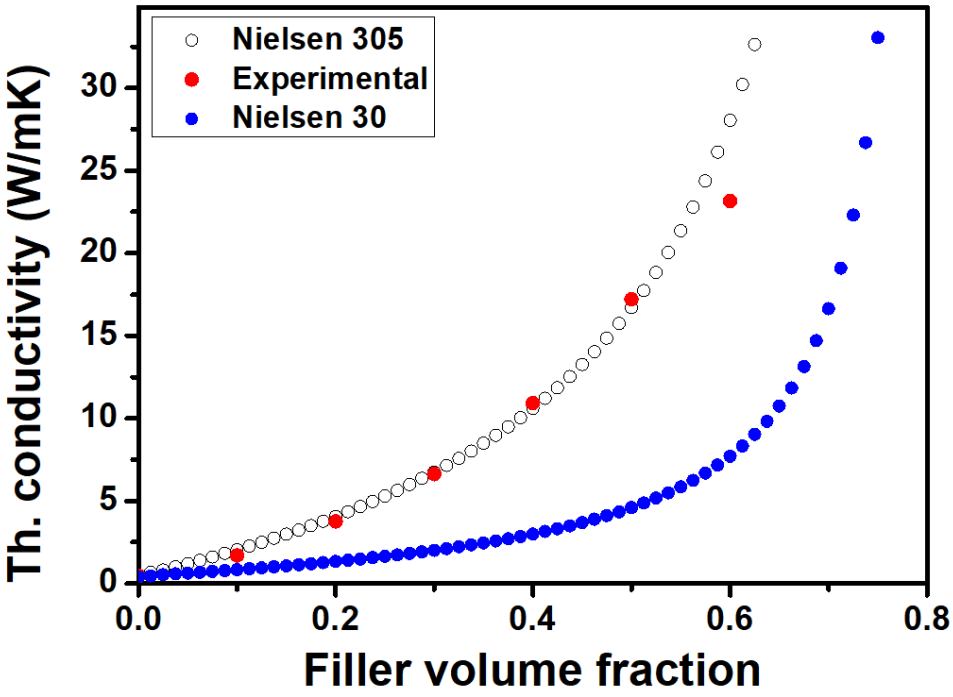

Figure S7. Experimental (red circles) and predicted thermal conductivity values for the BPH-cured LCER/h-BN composites calculated by the Nielson model when A = 30 (blue filled circles) and 305 (black open circles).

References

[1] Yeo, H.; Islam, A. M.; You, N.-H.; Ahn, S.; Goh, M.; Hahn, J. R.; Jang, S. G., Characteristic Correlation between Liquid Crystalline Epoxy and Alumina Filler on Thermal Conducting Properties. *Composites Science and Technology* **2017,** *141*, 99-105.

[2] Kim, Y. C.; Park, S.-J.; Lee, J.-R., Effects of N-Benzylpyrazinium Hexafluoroantimonate Concentration on Rheological Properties in Cationic Epoxy Cure System. *Polymer Journal* **1997,** *29*, 759-765.

[3] Hill, L.W., Dynamic Mechanical and Tensile Properties, J.V. Koleske (Ed.), Paint and Coating Testing Manual, ASTM, Philadelphia, **1995**, *46*, 534-546.

[4] Keenan, M. R., Autocatalytic Cure Kinetics from DSC Measurements: Zero Initial Cure Rate, *J. Appl. Polym. Sci*. **1987**, *33*, 1725-1734.

[5] Lee, J. Y.; Choi, H. K.; Shim, M. J.; Kim, S. W., Kinetic Studies of an Epoxy Cure Reaction by Isothermal DSC Analysis, *Thermochimica Acta*, **2000**, *343*, 111-117.

[6] Hayaty, M.; Beheshty, M. H.; Esfandeh, M., Isothermal Differential Scanning Calorimetry Study of a Glass/epoxy Prepreg, Polym. *Adv. Technol*. **2011**, *22*, 1001-1006.

[7] He, Y., Rapid Thermal Conductivity Measurement with a Hot Disk Sensor, Part 1. Theroretical Considerations, *Thermochimica Acta,* **2005**, 436, 122-129

[8] Agari, Y.; Ueda, A.; Nagai, S., Thermal Conductivity of a Polymer Composite. *Journal of Applied Polymer Science* **1993,** *49* (9), 1625-1634.

[9] Maxwell, J. C., *A* Treatise on Electricity and Magnetism. Dover: 1954.

[10] Cheng, S. C.; Vachon, R. I., The Prediction of the Thermal Conductivity of Two and Three Phase Solid Heterogeneous Mixtures. *International Journal of Heat and Mass Transfer* **1969,** *12* (3), 249-264.

[11] Nielsen, L. E., Generalized Equation for the Elastic Moduli of Composite Materials. *Journal of Applied Physics* **1970,** *41* (11), 4626-4627.

[12] Chung, S. L.; Lin, J. S., Thermal Conductivity of Epoxy Resin Composites Filled with Combustion Synthesized h-BN Particles. *Molecules* **2016,** *21* (5), 670.

[13] Corcione Carola, E.; Freuli, F.; Maffezzoli, A., The Aspect Ratio of Epoxy Matrix Nanocomposites Reinforced with Graphene Stacks. *Polymer Engineering & Science* **2012,** *53* (3), 531-539.

[14] Mortazavi, B.; Pereira, L. F. C.; Jiang, J.-W.; Rabczuk, T., Modelling Heat Conduction in Polycrystalline Hexagonal Boron-Nitride Films. *Scientific Reports* **2015,** *5*, 13228.

[15] Zhu, H.; Li, Y.; Fang, Z.; Xu, J.; Cao, F.; Wan, J.; Preston, C.; Yang, B.; Hu, L., Highly Thermally Conductive Papers with Percolative Layered Boron Nitride Nanosheets. *ACS Nano* **2014,** *8* (4), 3606-3613.

[16] Kimura, Y.; Wakabayashi, T.; Okada, K.; Wada, T.; Nishikawa, H., Boron Nitride as a Lubricant Additive. *Wear* **1999,** *232* (2), 199-206.

[17] Deepika; Li, L. H.; Glushenkov, A. M.; Hait, S. K.; Hodgson, P.; Chen, Y., High-Efficient Production of Boron Nitride Nanosheets via an Optimized Ball Milling Process for Lubrication in Oil. *Scientific Reports* **2014,** *4*, 7288.